Effect of Mo on microstructure, mechanical and corrosion properties of FeCrNiMnMo$_x$ high-entropy alloys

Xue-wei Xing, Jin-kang Hu, *Ying Liu, and Wei Li

Institute of Advanced Wear & Corrosion Resistant and Functional Materials, Jinan University, Guangzhou 510632, China

Abstract: Four FeCrNiMnMo$_x$ (x=0, 0.1, 0.3, 0.5, in molar ratio) high-entropy alloys (HEAs) were synthesized by vacuum arc melting to explore the potential impact of Mo on the microstructure, mechanical properties, and passivation and electrochemical behaviors in 0.5 M H$_2$SO$_4$ solution. The results display that the FeCrNiMn alloy exhibits a single face-centered cubic (FCC) structure while the microstructures of the FeCrNiMnMo$_{0.1}$, FeCrNiMnMo$_{0.3}$, and FeCrNiMnMo$_{0.5}$ alloys consist of the FCC and σ phase. The appear of the σ phase ascribed to the addition of Mo enhances the hardness and yield strength with the sacrifice of plasticity. The FeCrNiMnMo$_x$ HEAs achieve the maximum hardness of 414 HV$_{0.2}$ and the highest compressive yield strength of 830 MPa when x=0.5, but compressive fracture strain is lowered to 10.8%. X-ray photoelectron spectroscopy (XPS) and electrochemical analysis show that the passivation film in FeCrNiMnMo$_x$ alloy mainly consists of chromium oxides and molybdenum oxides. Mo has a beneficial effect on the corrosion resistance of the FeCrNiMnMo$_x$ HEAs in a 0.5 M H$_2$SO$_4$ solution by increasing the corrosion potential (E_{corr}) and decreasing the corrosion current density (I_{corr}) and passivation current density (I_{pass}). The FeCrNiMnMo$_{0.1}$ alloy shows the best corrosion resistance, mainly due to its passivation film consisting of a large proportion of chromium oxide (Cr$_2$O$_3$). More Mo additions promote the formation of the precipitate of σ phase and the matrix regions depleted Cr and Mo elements adverse to the resistance to preferential localized corrosion.

Keywords: high-entropy alloy; microstructure; mechanical properties; corrosion behavior; X-ray photoelectron spectroscopy (XPS)

CLC numbers: TG143.9; Document code: A; Article ID: 1672-6421(2022)06-464-09

*Ying Liu

Born in 1966, Associate Professor. Research interests: Preparation and optimization of microstructure and properties of metallic materials.

E-mail: liuying2000ly@163.com

Authors Xue-wei Xing and Jin-kang Hu contributed equally to this article.

1 Introduction

The recently developed high-entropy alloys (HEAs) have attracted wide interest and attention since put forward by Yeh et al. [1] in 2004 and have broken the bottleneck of conventional alloy design concept based on one or two principal components. High-entropy alloys, also namely the multicomponent alloys, are composed of at least five major or principal elements with each element having a concentration of 5%–35% and exhibiting a significant degree of mutual solubility to form disordered simple face-centered cubic (FCC), body-centered cubic (BCC) or hexagonal closed-packed (HCP) solid solution phases [2, 3], and some multi-phase microstructure containing intermetallic [4] or even amorphous phases [3]. Due to the unique multi-principal element compositions and the four core effects [5] including high-entropy effect, sluggish diffusion effect, severe lattice-distortion and cocktail effect, HEAs possess special properties including high strength/hardness, outstanding wear resistance, exceptional high-temperature strength, good structural stability, good corrosion and oxidation resistance [6], implying the potential application of HEAs in many fields.

The alloy element Mo has a great influence on the microstructure and mechanical properties of high-entropy alloys [7-13]. He et al. [7] evaluated the effect of a single element on the precipitation behavior of CoCrFeNi HEA, revealing that at 750 °C, the CoCrFeNi matrix can dissolve up to 3at.% Mo, and the small precipitate of σ or μ phase rich in Mo and Cr appeared when the Mo content was higher in the CoCrFeNi alloy. Liu et al. [8] reported that the precipitation of hard σ and μ intermetallic compounds greatly strengthened the $CoCrFeNiMo_{0.3}$ HEA, which exhibited a tensile strength of up to 1.2 GPa and good ductility of about 19%. Liu et al. [9] evaluated the friction and wear properties of the $FeCoCrNiMo_x$ (x=0–1.5) HEAs and found the wear resistance improved with the increase of Mo until x=1 and $FeCoCrNiMo_1$ alloy presented a lower average friction coefficient and wear rate among the tested alloys, attributed to the desired types, amount, size, distribution of the hard σ and μ phases in the ductile FCC solid solution. Dong et al. [10] revealed that the increase of a certain addition amount of Mo in $AlCrFeNiMo_x$ (x=0, 0.2, 0.5, 0.8, 1.0) HEAs caused the two BCC phases transform to one BCC phase plus FeCrMo-type sigma phase structure and significantly improved the hardness from 472.4 to 911.5 HV. With the increase of Mo contents from x=0 to x=0.5, the yield strength increased substantially from 1,406.2 MPa to 1,748.6 MPa. The $AlCrFeNiMo_{0.2}$ had the highest fracture strength of 3,222 MPa and plastic strain of 0.287. It is worth noting that Mo has the potential to increase the corrosion property of HEAs. Dai et al. [11] reported that the $CoCrFeNiMo_x$ HEAs with low Mo content exhibited a single FCC structure, and pitting corrosion was observed when immersed in the sodium chloride solution. However, when the Mo content increased from x=0.3 to x=0.6, the (Mo, Cr) phase precipitates formed, which affected the corrosion resistance of the alloys. Electrochemical behaviors of $FeCoCrNiMo_x$ HEAs in sulfuric acid were also investigated by Dai et al [12]. It was manifested that $FeCoCrNiMo_x$ HEAs formed a double passive film in sulfuric acid solution, and the composition and passivation ability of the passive film were determined by the Cr/Mo ratio. Chou et al. [13] discovered that adding Mo to the $Co_{1.5}CrFeNi_{1.5}Ti_{0.5}$ alloy can improve the corrosion behavior so that the alloy can have a wide passivation region of 1.43 V in 1 M NaCl, suggesting that any pitting corrosion was prevented. Meanwhile, corrosion resistance of the CoCrFeNi $(W_{1-x}Mo_x)$ (x=0, 0.5) HEA coatings in 3.5% NaCl solution was enhanced remarkably by Mo addition [14].

As Co is expensive, the Co-free HEAs are interesting. As less is still known about the properties of FeCrNiMnMo series HEAs, the present work aims to study the microstructure, mechanical properties, corrosion resistance and passivation films of as-cast $FeCrMnNiMo_x$ HEAs.

2 Materials and methods

$FeCrNiMnMo_x$ (x=0, 0.1, 0.3, 0.5, in molar ratio) alloys were synthesized by arc melting in a water-cooled copper crucible under a Ti-gettered high-purity argon atmosphere. The pure metal particles of Fe (99.9%), Cr (99.9%), Ni (99.9%), Mn (99.9%), and Mo (99.9%) were used as raw materials. All ingots were flipped and remelted 7 times under electromagnetic stirring to ensure homogeneity. The size of the ingot was approximately $\Phi35$ mm×12 mm. The crystal structures were analyzed by X-ray diffraction (XRD) (Ultima IV, Rigaku, Tokyo, Japan) with the 2θ ranging from 20° to 100° at a speed of 8°·min⁻¹. The structure, chemical composition of the alloy, and the energy spectrum were observed and analyzed using a Nova Nano SEM430 scanning electron microscope (SEM). The hardness of the samples was measured with an HVS-1000 hardness tester at a load of 200 GF. The compressive test was carried out on an MTS E45.305 micro control electronic universal testing machine. The size of the compressive test specimen was $\Phi5$ mm×10 mm and the initial ram speed of the compression test was 1 mm·min⁻¹. The corrosion resistance of the $FeCrNiMnMo_x$ alloys was examined under 0.5 M sulfuric acid (H_2SO_4) at room temperature, and the electrochemical testing was conducted on a CHI7601 electrochemical workstation. A saturated calomel electrode (SCE) was used as the reference electrode, E=0.2415 V vs. SCE (V_{SCE}), and the platinum plate electrode was used as the auxiliary electrode. The $FeCrNiMnMo_x$ (x=0, 0.1, 0.3, 0.5) alloy samples sealed with a sealing glue were treated as the working electrode, with only the analysis surface exposed. The analysis surface was mechanically ground to 3000 grit using SiC water sandpaper. After polishing, it was subjected to ultrasonic cleaning with ultrapure water and absolute ethanol in sequence, before being dried by cold air and stored in a vacuum desiccator for use. When measuring the potentiodynamic polarization curve, the open circuit potential (OCP) was operated continuously for 1 h to avoid voltage disturbance. Potentiodynamic polarization curves were tested and plotted at a scan rate of 1 mV·s⁻¹ beginning from −1.2 V_{SCE} to a final potential of 1.5 V_{SCE} in sulfuric acid versus the open current potential. After the electrochemical experiment, the alloy was washed with distilled water in an ultrasonic cleaner and blow-dried. The corroded surfaces were analyzed by SEM. The composition of the passivation film developing on the surface of the alloy sample by immersion in 0.5 M H_2SO_4 for 24 h was analyzed by X-ray photoelectron spectroscopy (XPS, ESCALAB 250 xi, Thermo-VG Scientific, MA, USA) with an Al Kα radiation (1486.6 eV).

3 Results and discussion

3.1 Crystal structure

Figure 1 shows the XRD patterns of the four HEA samples. It can be found that the FeCrNiMn alloy exhibits a single face-centered cubic (FCC) structure, which can be identified as (Fe,Ni)-type solid solution phase, while $FeCrNiMnMo_{0.1}$, $FeCrNiMnMo_{0.3}$, and $FeCrNiMnMo_{0.5}$ alloys exhibit FCC and σ phases. The existence of the σ phase should be attributed to the introduction of Mo. The spectrum intensity of the σ phase is positively correlated with Mo content, as shown in Fig. 1(a). The strengthening effect of solution can be impacted

by Mo and the more Mo-containing HEAs will have a larger lattice constant because of the larger atomic radius of Mo. The (200) peak of the FCC phase shifts to the lower 2θ with the Mo content increase from $x=0$ to $x=0.5$, as shown in Fig. 1(b). This shift is due to the variation of lattice parameters of the FCC phase, which are estimated to be 0.6498, 0.6587, 0.6631, and 0.6690 nm for the FeCrNiMnMo$_x$ alloy at $x=0$, 0.1, 0.3, 0.5, respectively. Since the atomic radius of Mo (140 pm) is larger compared to Fe (1.24 pm), Cr (128 pm), Ni (125 pm), and Mn (124 pm), the effect of alloy solid solution strengthening can be achieved.

The phase formation and structural stability in HEAs can be predicted by the thermodynamic parameter ΔH_{mix} (mixing enthalpy), δ (atomic size difference), ΔS_{mix} (mixing entropy) and Ω (solid solution forming ability) [2, 15]. The solid solution phases only form when the parameters meet the ΔH_{mix} and δ criterion (-15 kJ·mol^{-1} $\leq \Delta H_{\text{mix}} \leq 5$ kJ·mol^{-1} and $\delta \leq 6.5\%$) as well as the Ω and δ criterion ($\Omega \geq 1.1$ and $\delta \leq 6.6\%$) [15]. Furthermore, Guo et al. [3] concluded that larger valence electron concentration (VEC) (≥ 8) favors the formation of FCC solid solutions, while smaller VEC (<6.87) favors the formation of BCC solid solutions. The following equations were used:

$$\Delta H_{\text{mix}} = 4\sum_{i=1, i \neq j}^{n} \Delta H_{ij}^{\text{mix}} C_i C_j \tag{1}$$

$$\Delta S_{\text{mix}} = -R\sum_{i=1}^{n} C_i \ln C_i \tag{2}$$

$$\Omega = \frac{T_m \Delta S_{\text{mix}}}{\left| \Delta H_{\text{mix}} \right|} \tag{3}$$

$$\delta = \sqrt{\sum_{i=1}^{n} C_i \left(1 - r_i / \bar{r}\right)^2} \tag{4}$$

where C_i, C_j are the atomic fraction of element i and j in the alloy; R is the gas constant; T_m represents the melting point of the n-component alloy; r_i represents the radius of the i element, $\bar{r}$ is the average atomic radius. Table 1 lists the calculated parameters Ω, ΔH_{mix}, ΔS_{mix}, and VEC of the FeCrNiMnMo$_x$ HEAs. For the studied FeCrNiMnMo$_x$ alloys, the calculated Ω is 5.21–7.12, ΔH_{mix} is $-4 - -3.56$ kJ·mol^{-1}, ΔS_{mix} is 11.52–13.14 J·K^{-1}·mol^{-1}, δ is 3.57%–4% and VEC is 7.55–7.75. According to the above criterion favoring the formation of solid solutions, not only FCC solid solution would form in the alloys.

The precipitation of the σ phase is ascribed to the segregation of Mo on a large extent. Though the above mentioned thermodynamic parameters can predict the solid solution formation, they fail to predict the likelihood of the σ phase formation. However, Tsai et al. [16] proposed that σ phase is prone to form in Cr-containing HEAs when VEC ranges from 6.88 to 7.84, and the tendency to form σ phase in an austenitic stainless steel can be known from the equivalent chromium content (ECC) equation [13]: ECC = 1%Cr + 0.31% Mn + 1.76% Mo + 0.97% W + 2.02% V + 1.58% Si + 2.44% Ti + 1.7% Nb + 1.22% Ta – 0.266% Ni – 0.177% Co. If the ECC exceeds 17wt.%–18wt.%, the σ phase likely to form in steel. In this study, the ECC of FeCrNiMnMo$_x$ ($x=0$, 0.1, 0.3, 0.5) is 23.1wt.%, 30.4wt.%, 41.6wt.% and 51.1wt.%, respectively. Therefore, Mo can promote the formation of σ phase.
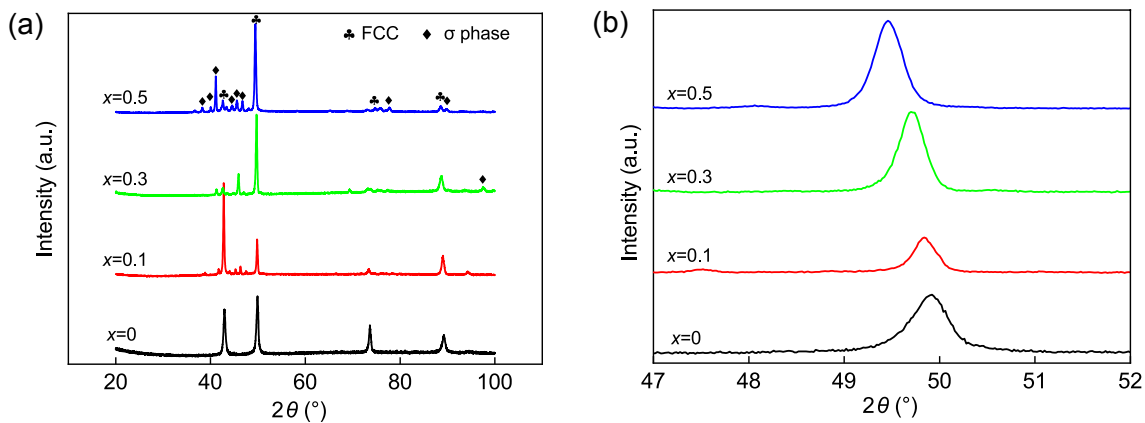

Fig. 1: XRD patterns of FeCrNiMnMo$_x$ HEAs (a), and detailed (200) peaks of FCC phase (b)

Table 1: Parameters of FeCrNiMnMo$_x$ HEAs

Alloy	ΔH_{mix} (kJ·mol^{-1})	ΔS_{mix} (J·K^{-1}·mol^{-1})	T_m (K)	Ω	δ (%)	VEC
FeCrNiMn	–4	11.52	1,809.5	5.21	3.57	7.75
FeCrNiMnMo$_{0.1}$	–3.9	12.19	1,836.7	5.74	3.67	7.71
FeCrNiMnMo$_{0.3}$	–3.73	12.82	1,888.3	6.49	3.88	7.64
FeCrNiMnMo$_{0.5}$	–3.56	13.14	1,930.3	7.12	4.02	7.55

3.2 Microstructure

Figure 2 demonstrates the microstructure of the FeCrNiMnMo$_x$ HEAs with different contents of Mo. The FeCrNiMn alloy [Fig. 2(a)] has a homogeneous single FCC phase grain structure. With the addition of Mo, the σ phase particle appears in FeCrNiMnMo$_{0.1}$, FeCrNiMnMo$_{0.3}$ and FeCrNiMnMo$_{0.5}$ alloys, and exists in dendritic regions. With the Mo content increases, the σ phase grows up, so the particle size of σ phase increases. Figure 3 displays the relationship between the volume fraction of σ phase and Mo content in the HEAs. Without Mo addition, only the FCC phase, rather than the σ phase, exists. As Mo$_{0.1}$ is added, a small amount of the σ phase is formed. The volume fraction of σ phase increases with the increasing content of Mo.
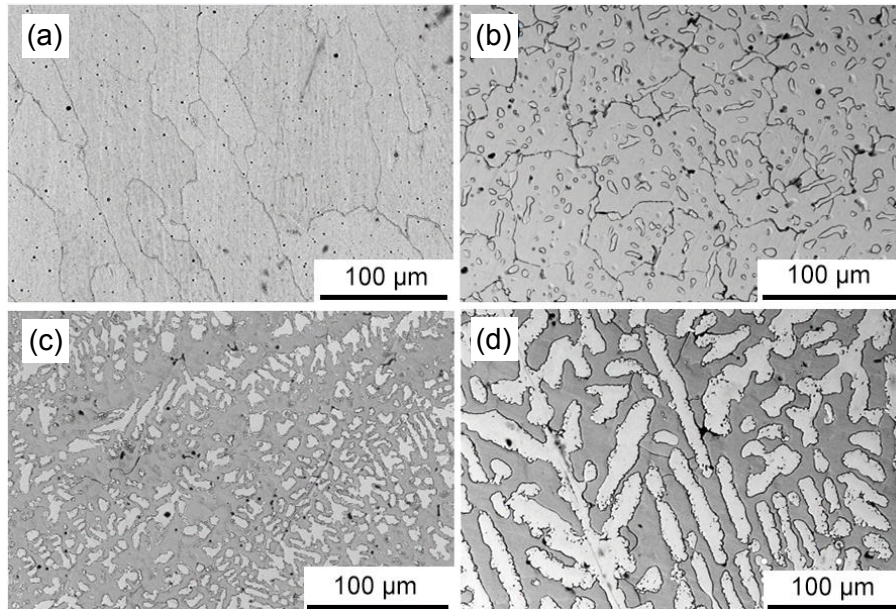

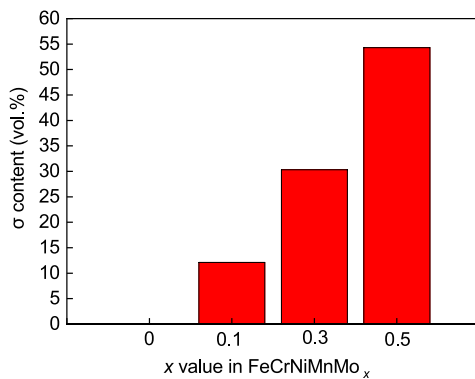**Fig. 2: Microstructure of the FeCrNiMnMo$_x$ HEAs: (a) x=0; (b) x=0.1; (c) x=0.3; (d) x=0.5**

Fig. 3: Volume fraction of σ in experimental alloys

Figure 4 shows the EDS maps of the element distribution for the FeCrNiMnMo$_{0.3}$ HEA, and the EDS analysis of the marked positions in dendrite (DR) and inter-dendrite (ID) regions of the alloy is given in Table 2. It can be observed the distribution of the elements is not homogeneous from DR to ID regions and more serious elemental segregation of Mo, Mn and Ni exists in the dendrite regions. According to EDS results, the σ phase region (DR) is rich in Fe, Cr and Mo elements, while the matrix FCC phase region (ID) consists of Mn and Ni-rich phase, in which the Fe is evenly distributed. Therefore, the σ phase is formed mainly by the segregation of Mo and Cr.

3.3 Mechanical properties

Figure 5(a) displays the hardness of the FeCrNiMnMo$_x$ HEAs. It can be seen that the microhardness is increased with the content of Mo increases. The microhardness of FeCrNiMnMo$_{0.5}$ HEA is up to 414 HV, which is about 2 times higher than that of FeCrNiMn alloy. The increasing hardness for FeCrNiMnMo$_{0.1}$ may be related to the lattice distortion and solid solution strengthening that results from the addition of Mo atoms into the alloy [6-7]. The obviously increasing hardness in FeCrNiMnMo$_{0.3}$ and FeCrNiMnMo$_{0.5}$ alloys is mainly due to the increasing volume fraction of the hard σ phase, which exerts the second phase strengthening [8-9]. Figure 5(b) shows the room temperature compression stress-strain curves of FeCrNiMnMo$_x$ alloys. FeCrNiMn and FeCrNiMnMo$_{0.1}$ HEAs show extremely high ductility without fractures that occur during the testing. As the content of Mo increases higher, the ductility of the HEA decreases but the yield strength increases; the compressive strength increases firstly and then declines. The FeCrNiMnMo$_{0.3}$ and FeCrNiMnMo$_{0.5}$ HEAs have compressive yield strength of 810 MPa and 830 MPa, compressive ultimate strength of 1,280 MPa and 1,040 MPa, and fracture strain of 14.9% and 10.8%, respectively. Due to solid solution strengthening, the FeCrNiMnMo$_{0.1}$ alloy exhibits high strength and plasticity. When the second phase is introduced and evenly distributed in the matrix phase with finely dispersed particles, a significant strengthening effect will occur. As the content of Mo increases, the second phase (σ phase) becomes larger and denser. The σ phase belongs to the Topological Close-Packed (TCP) group of structures, the large misalignments between them and the FCC lattice will lead to
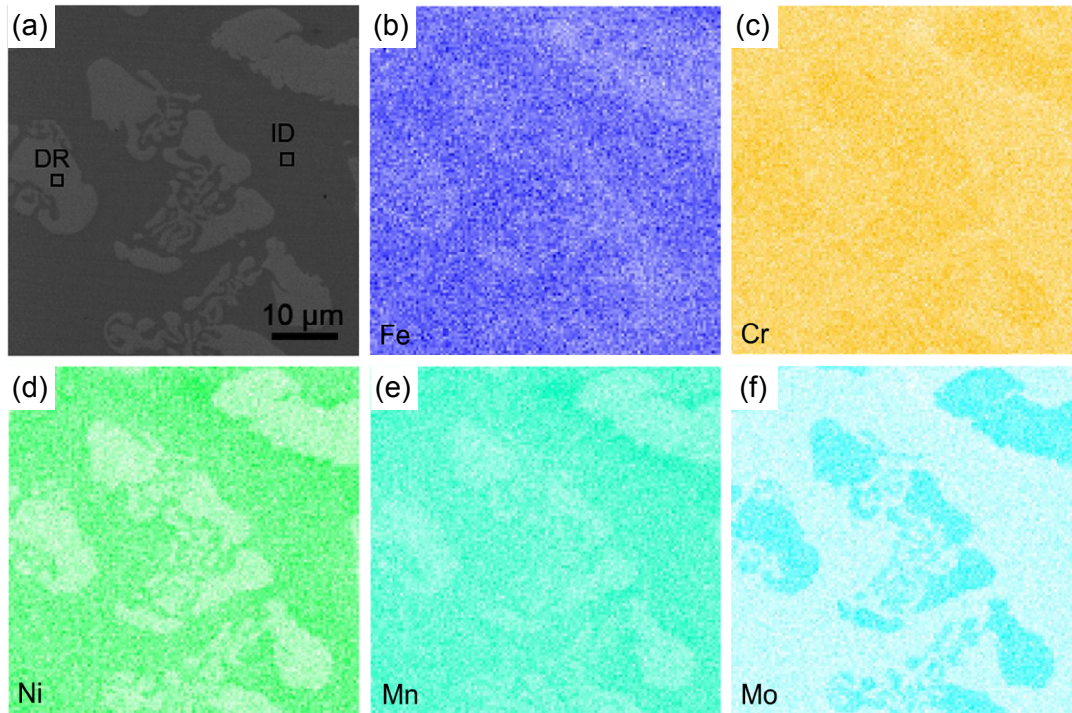
Fig. 4: EDS maps of FeCrNiMnMo₀.₃ HEA BSD image (a), element distribution of Fe (b), Cr (c), Ni (d), Mn (e), and Mo (f), respectively

Table 2: EDS analysis results of FeCrNiMnMo$_{0.3}$ alloy (at.%) in DR and ID regions in Fig. 4(a)

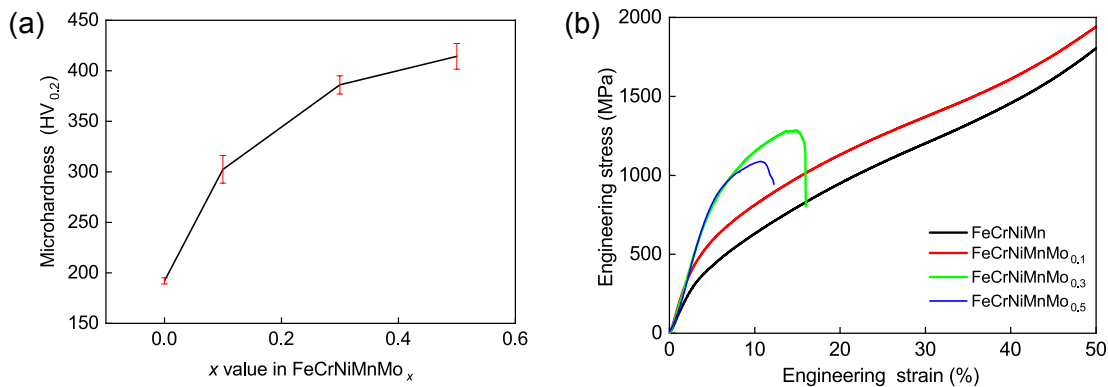| Element	Fe	Cr	Ni	Mn	Mo
DR	23.06	29.15	13.46	15.18	19.15
ID	20.74	13.75	32.10	27.42	5.99

Fig. 5: Mechanical properties of FeCrNiMnMo$_x$ HEAs: (a) microhardness; (b) engineering stress-strain curves

the accumulation of dislocations at the interface, and the stress concentration occurs. Thus, cracking is apt to generate during the compression, and the HEAs with greater content of Mo will turn fragile.

3.4 Potentiodynamic polarization curves and SEM photomicrographs of corroded surfaces

Figure 6(a) shows the potential polarization curves of FeCrNiMnMo$_x$ (x=0, 0.1, 0.3, 0.5) alloys in 0.5 M H$_2$SO$_4$ solution, and Table 3 gives the corrosion characteristics derived from Fig. 6(a) including corrosion potential (E_{corr}), corrosion current density (I_{corr}), primary passivation current density (I_{pp}),

passivation current density (I_{pass}) and the breakdown potential (E_b). It can be observed that the corrosion potential of Mo-containing alloys increases dramatically, more than 50 mV, and the corrosion current density decreases rapidly at first in the FeCrNiMnMo$_{0.1}$ alloy, and then rises up in the FeCrNiMnMo$_{0.3}$ alloy but slightly down in the FeCrNiMnMo$_{0.5}$ alloy, which still shows a decreased order of magnitude compared to FeCrNiMn alloy. The case existing in the primary passivation potential (E_{pp}) is similar to E_{corr}, but the E_b is almost stable, and the cases of I_{pp} and I_{pass} are similar to I_{corr} in Mo-containing alloys. The Mo addition has little effect on the width of the passive region for the FeCrNiMnMo$_x$ alloys. As Fe and Mn
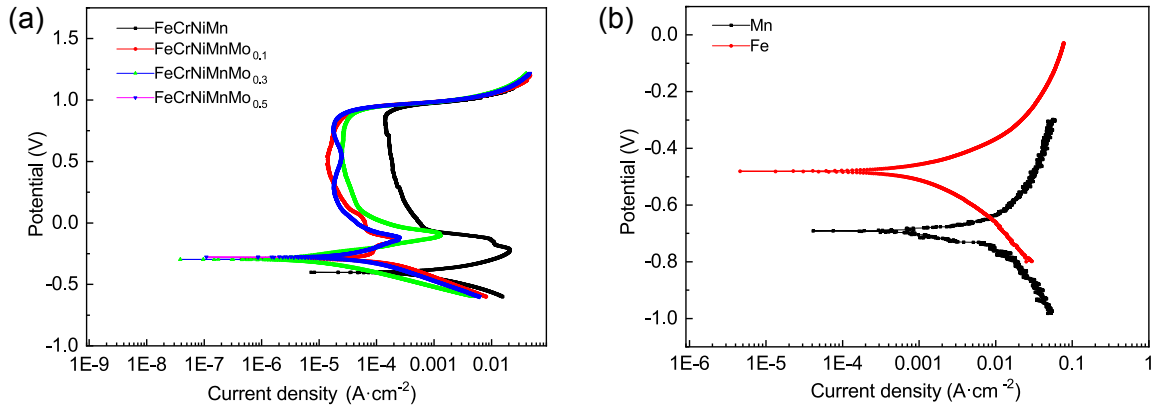
Fig. 6: Polarization curves of FeCrNiMnMo$_x$ HEAs, Fe and Mn in 0.5 M H$_2$SO$_4$: (a) FeCrNiMnMo$_x$ HEA; (b) Fe, Mn

Table 3: Electrochemical parameters of FeCrNiMnMo$_x$ alloys in 0.5 M H$_2$SO$_4$ solution

Sample	E_{corr} (V)	I_{corr} (A·cm^{-2})	E_{pp} (V)	I_{pp} (A·cm^{-2})	E_b (V)	I_{pass} (A·cm^{-2})
FeCrNiMn	–0.40	8.85E-4	–0.22	2.22E-2	0.88	1.40E-4
FeCrNiMnMo$_{0.1}$	–0.34	6.77E-6	–0.15	2.07E-4	0.88	1.35E-5
FeCrNiMnMo$_{0.3}$	–0.27	5.66E-5	–0.10	1.27E-3	0.88	2.47E-5
FeCrNiMnMo$_{0.5}$	–0.28	3.00E-5	–0.12	2.55E-4	0.89	1.78E-5

have no obvious passive region in the potential polarization curve [Fig. 6(b)], the Mo addition inhibits the dissolution of Fe and Cr by reducing I_{pass}. The higher E_{corr}, lower I_{corr} and I_{pass} of the Mo-containing alloy suggest that a certain amount of Mo has a beneficial effect on the corrosion resistance. The FeCrNiMnMo$_{0.1}$ alloy exhibits the best corrosion resistance capacity among the four HEAs in H$_2$SO$_4$ environment.

SEM images of specimens after potentiodynamic polarization tests in a 0.5 M H$_2$SO$_4$ solution are shown in Fig. 7. In Fig. 7(a), local corrosion, pitting, and spalling can be observed in the FeCrMnNi alloy. The corrosion morphology becomes smoother on the FeCrNiMnMo$_{0.1}$ alloy though there are few micropores due to the peeling of the σ phase. The galvanic corrosion can be seen in the HEAs with more Mo content. The microstructure can obviously affect the corrosion resistance. Uniform microstructure and the little or non-segregation of the composition can inhibit the inhomogeneity of electrochemical performance among phases and grain boundaries. As can be seen from the above-mentioned microstructure, the FCC phase and the σ phase demarcate more clearly with the increasing Mo element. Selective dissolution and pitting occur on the FCC phase. According to EDS analysis in Fig. 4, Cr and Mo are enriched in the σ phase but depleted in the FCC phase region. The Mo addition improves the corrosion resistance by improving the quality of the passive film, but more Mo addition leads to more precipitation, and the element segregation of Cr and Mo may adverse to the resistance to preferential localized corrosion. Therefore, FeCrNiMnMo$_{0.3}$ and FeCrNiMnMo$_{0.5}$ alloys have a lower corrosion resistance than FeCrNiMnMo$_{0.1}$ alloy.

3.5 Evaluation of protective ability of passive films by XPS

The chemical composition of the passivation film on FeCrNiMnMo$_x$ alloys was studied by XPS. Figure 8 shows the spectra in detail of Cr2p, Mo3d, Ni2p, Fe2p, and Mn2p in the passivation film of FeCrNiMnMo$_{0.1}$ alloy immersion in the 0.5 M H$_2$SO$_4$ solution for 24 h. Four oxide constituent peaks fit in Cr2p spectrum are metal Cr2p1/2-Cr2p3/2 and Cr$_2$O$_3$2p1/2-Cr$_2$O$_3$2p3/2, respectively. Among them, Cr$_2$O$_3$ is the dominant chemical state of the chromium ionization in the passive film. In the Mo3d spectrum, there are one peak of Mo3d3/2 of metallic Mo and double Mo^{6+}3d peaks of MoO$_3$3d3/2 and MoO$_3$3d5/2, in which two MoO$_3$ peaks are stronger. In the Ni2p spectrum, there are two transition states of the pure Ni2p3/2 and NiO2p3/2 in the passivation film. However, it mainly exists in the form of metallic Ni, because the intensity and area of the peaks representing nickel oxide are small. The Fe2p spectrum consists of FeO, Fe$_2$O$_3$ and mostly Fe, implying there is little iron oxide in the passivation film. Only the metal-transitioned Mn is found in the Mn2p transition. In combination with the Fe and Mn polarization curves [Fig. 6(b)], it can be estimated that Fe and Mn do not contribute to the corrosion passivation film formed in the sulfuric acid solution. The main components of the passivation film are oxides of chromium and molybdenum.

Figure 9 shows the XPS spectra of Cr2p3/2 and Mo3d in FeCrNiMnMo$_x$ alloy passivation film immersing in 0.5 M H$_2$SO$_4$ solution for 24 h, and Table 4 gives the peak areas of Cr^{3+}, Cr, Mo$^{4+, 6+}$, and Mo in the passivation film. It can be found that the Cr (2p) spectrum of the FeCrNiMnMo$_x$ alloy has two peaks at
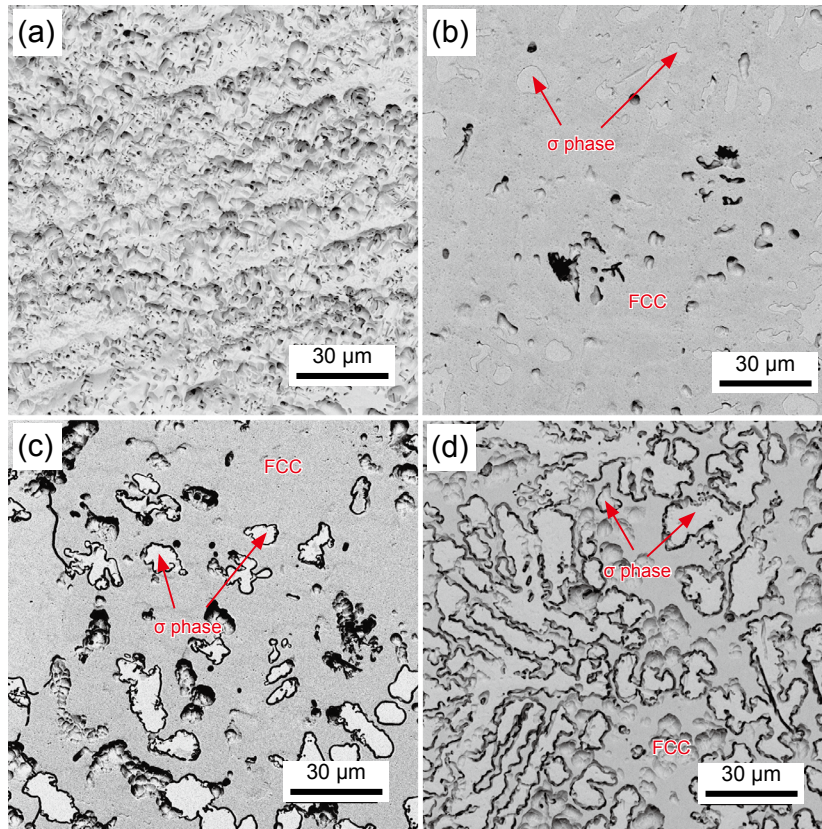
Fig. 7: SEM images of corroded surface after polarization testing in 0.5 M H₂SO₄: (a) FeCrNiMn;
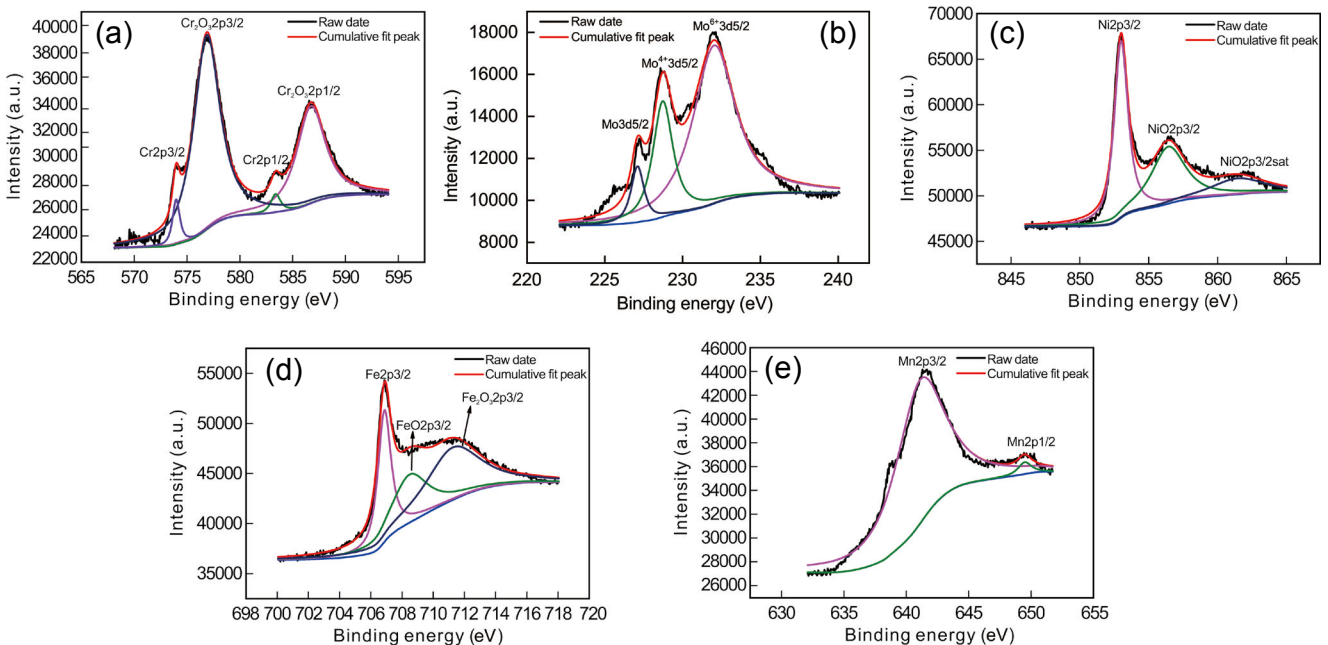**(b) FeCrNiMnMo₀.₁; (c) FeCrNiMnMo₀.₃; (d) FeCrNiMnMo₀.₅**

Fig. 8: Detailed XPS sputtering spectra of Cr2p (a), Mo3d (b), Ni2p (c), Fe2p (d), and Mn2p (e) in the passivation
film of FeCrNiMnMo₀.₁ alloy immersion in 0.5 M H₂SO₄ solution for 24 h

586.40 eV (2p) and 576.80 eV (2p) in Fig. 8(a) and Figs. 9(a, b), indicating the presence of chromium oxide (Cr_2O_3). The area and strength of Cr_2O_3 increase firstly and then decrease with the addition of Mo, and the area and intensity of Cr_2O_3 are the largest in FeCrNiMnMo₀.₁ alloy. According to Table 4, further addition of Mo no longer increases the area and strength of Cr_2O_3. The

Mo (3d) spectra for the FeCrNiMnMo₀.₁ alloy in Fig. 8(b) and FeCrNiMnMo₀.₃ alloy in Fig. 9(c) indicate the formation of molybdenum oxide in different valence states, which can improve the resistance to attack from the aggressive ions [17, 18]. Naturally, the corrosion resistance of a material depends on the composition of the passivation film formed on the surface.

Research demonstrates that Cr_2O_3 is responsible for and plays a crucial role in the enhancement of corrosion resistance [19], so, the moderate addition of Mo is effective in promoting the development of Cr_2O_3 and enhancing the stability of the passive film by maintaining a large Cr_2O_3 proportion through the solution of Mo into the matrix and precipitation of Mo oxide, thus the passivation film formed in the $FeCrNiMnMo_{0.1}$ alloy can be more effective than that in FeCrNiMn, $FeCrNiMnMo_{0.3}$, and $FeCrNiMnMo_{0.5}$ alloys.
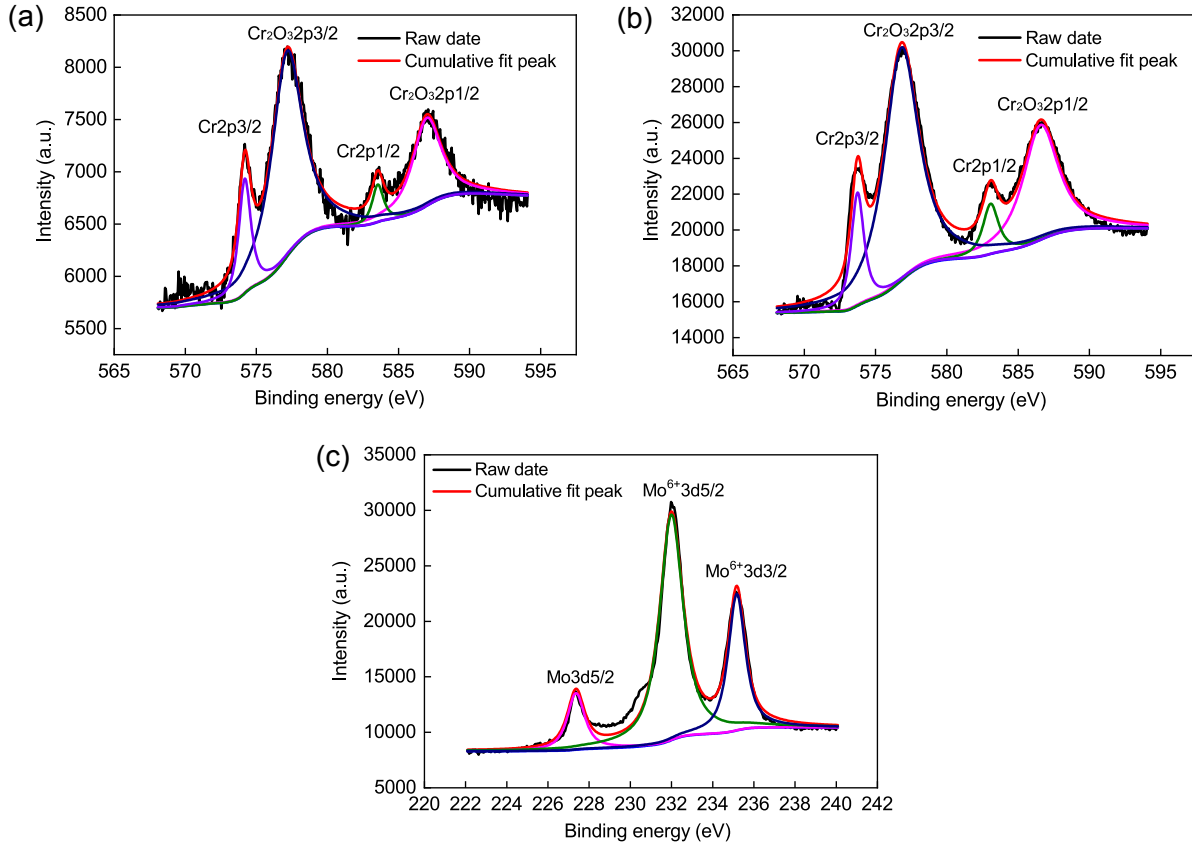

Fig. 9: XPS spectra of Cr2p3/2 and Mo3d in $FeCrNiMnMo_x$ alloy passivation film: (a) x=0 (Cr2p); (b) x=0.3 (Cr2p); (c) x=0.3 (Mo3d)

Table 4: Peak areas of Cr^{3+}, Cr, $Mo^{4+, 6+}$, and Mo in passivation filming of $FeCrNiMnMo_x$ alloys

Alloy	Cr^{3+}	Cr	$Mo^{4+, 6+}$	Mo
FeCrNiMn	6,774.69	4,553.40	–	–
$FeCrNiMnMo_{0.1}$	76,102.97	19,065.26	34,465.66	2,995.77
$FeCrNiMnMo_{0.3}$	46,730.55	11,408.96	51,042.18	6,903.41

4 Conclusions

(1) The FeCrNiMn alloy has a single FCC phase structure, while $FeCrNiMnMo_{0.1}$, $FeCrNiMnMo_{0.3}$, and $FeCrNiMnMo_{0.5}$ HEAs show FCC + σ phase dendritic structure.

(2) Mo can improve the hardness and yield strength of $FeCrNiMnMo_x$ alloys, but decrease the ductility. $FeCrNiMoMo_{0.5}$ HEA has the highest hardness of up to 414 HV, the highest compressive yield strength of 830 MPa, and the lowest fracture strain of 10.8%.

(3) Mo can effectively improve the corrosion resistance of the FeCrNiMn alloy in a 0.5 M H_2SO_4 solution by increasing the corrosion potential and decreasing the corrosion current density and passivation current density greatly. The passivation film on the $FeCrNiMnMo_x$ alloy is mainly composed of chromium oxides and molybdenum oxides. A certain amount of Mo can improve the protective ability of the passivation film, and $FeCrNiMnMo_{0.1}$ has the best corrosion resistance.

References

[1] Yeh J W, Chen S K, Lin S J, et al. Nanostructured high-entropy alloys with multiple principal elements: Novel alloy design concepts and outcomes. Advanced Engineering Materials, 2004, 6: 299–303.

[2]   Yang X, Zhang Y. Prediction of high-entropy stabilized solid-solution in multi-component alloys. Materials Chemistry and Physics, 2012, 132(2−3): 233−238.

[3]   Guo S, Liu C T. Phase stability in high entropy alloys: Formation of solid-solution phase or amorphous phase. Progress in Natural Science: Materials International, 2011, 21(6): 433−446.

[4]   Lua Y P, Dong Y, Jiang H, et al. Promising properties and future trend of eutectic high entropy alloys. Scripta Materialia, 2020, 187: 202−209.

[5]   Yeh J W. Recent progress in high entropy alloys. Annales De Chimie – Science des Materiaux, 2006, 31: 633−648.

[6]   Miracle D B, Senkov O N. A critical review of high entropy alloys and related concepts. Acta Materialia, 2017, 122: 448−511.

[7]   He F, Wang Z J, Han B, et al. Solid solubility, precipitates, and stacking fault energy of microalloyed CoCrFeNi high entropy alloys. Journal of Alloys and Compounds, 2018, 769: 490−502.

[8]   Liu W H, Lu Z P, He J Y, et al. Ductile CoCrFeNiMo$_x$ high entropy alloys strengthened by hard intermetallic phases. Acta Materialia, 2016, 116, 332−342

[9]   Liu Y, Xie Y X, Cui S G, et al. Effect of Mo element on the mechanical properties and tribological responses of CoCrFeNiMo$_x$ high-entropy alloys. Metals, 2021, 11(3): 486.

[10] Dong Y, Lu Y P, Kong J R, et al. Microstructure and mechanical properties of multi-component AlCrFeNiMo$_x$ high-entropy alloys. Journal of Alloys and Compounds, 2013, 573: 96−101.

[11] Dai C D, Zhao T L, Du C W, et al. Effect of molybdenum content on the microstructure and corrosion behavior of FeCoCrNiMo$_x$ high-entropy alloys. Journal of Materials Science & Technology, 2020, 46: 64−73.

[12] Dai C D, Luo H, Li J, et al. X-ray photoelectron spectroscopy and electrochemical investigation of the passive behavior of high entropy FeCoCrNiMo$_x$ alloys in sulfuric acid. Applied Surface Science, 2020, 499: 143903.

[13] Chou Y L, Yeh J W, Shih H C. The effect of molybdenum on the corrosion behaviour of the Co$_{1.5}$CrFeNi$_{1.5}$Ti$_{0.5}$Mo$_x$ high-entropy alloys in aqueous environments. Corrosion Science, 2010, 52: 2571−2581.

[14] Shang C Y, Axinte E, Sun J, et al. CoCrFeNi(W$_{1-x}$Mo$_x$) high-entropy alloy coatings with excellent mechanical properties and corrosion resistance prepared by mechanical alloying and hot pressing sintering. Materials Design, 2017, 117: 193−202.

[15] Zhang Y, Zhou Y J, Lin J P, et al. Solid-solution phase formation rules for multi-component alloys. Advanced Engineering Materials, 2010, 10(6): 534−538.

[16] Tsai K Y, Tsai M H, Yeh J W. Sluggish diffusion in CoCrFeMnNi high-entropy alloys. Acta Materialia, 2013, 61: 4887−4897.

[17] Pardo A, Merino M C, Coy A E, et al. Effect of Mo and Mn additions on the corrosion behaviour of AISI 304 and 316 stainless steels in H$_2$SO$_4$. Corrosion Science, 2008, 50(3): 780−784.

[18] Bojinov M, Fabricius G, Laitinen T, et al. Influence of molybdenum on the conduction mechanism in passive films on iron-chromium alloys in sulphuric acid solution. Electrochimica Acta, 2001, 46(9): 1339−1358.

[19] Sugimoto K, Sawada Y. Cheminform abstract: The role of molybdenum additions to austenitic stainless steels in the inhibition of pitting in acid chloride solutions. Corrosion Science, 1977, 17(5): 425−445.